Chemistry
A European
Journal

Chemistry Europe
European Chemical Societies Publishing

Accepted Article

Title: Influence of Amide Connectivity on the Hydrogen Bond Directed Self-Assembly of [n.n]Paracyclophanes

Authors: Will R. Henderson, Ajeet Kumar, Khalil A. Abboud, and Ronald K. Castellano

To be cited as: *Chem. Eur. J.* 10.1002/chem.202003909

Link to VoR: https://doi.org/10.1002/chem.202003909

WILEY-VCH

10.1002/chem.202003909

WILEY-VCH

FULL PAPER

Influence of Amide Connectivity on the Hydrogen Bond Directed Self-Assembly of [n.n]Paracyclophanes

Will R. Henderson, Ajeet Kumar, Khalil A. Abboud, Ronald K. Castellano*[a]

Dedicated to Prof. William R. Dolbier, Jr. for his contributions to cyclophane chemistry and the University of Florida.

[a] W. R. Henderson, A. Kumar, Dr. K. A. Abboud, Prof. R. K. Castellano
George & Josephine Butler Polymer Research Laboratory, Center for Macromolecular Science & Engineering
Department of Chemistry, P.O. Box 117200
University of Florida
Gainesville, Florida, 32611 (USA)
E-mail: castellano@chem.ufl.edu

Supporting information (molecular synthesis and characterization; NMR, IR, UV-Vis, and X-ray characterization of assembly; computational details) and the ORCID identification number(s) for the author(s) of this article is given via a link at the end of the document.

Abstract: Reported here is the synthesis and self-assembly characterization of [n.n]paracyclophanes (**[n.n]pCps**, n = 2, 3) equipped with anilide hydrogen bonding units. These molecules differ from previous self-assembling [n.n]paracyclophanes (**[n.n]pCps**) in the connectivity of their amide hydrogen bonding units (*C*-centered/carboxamide vs. *N*-centered/anilide). This subtle change results in a ~30-fold increase in the elongation constant for the **[2.2]pCp**-4,7,12,15-tetraanilide (**[2.2]pCpNTA**) compared to previously reported **[2.2]pCp**-4,7,12,15-tetracarboxamide (**[2.2]pCpTA**), and a ~300-fold increase in the elongation constant for the **[3.3]pCp**-5,8,14,17-tetraanilide (**[3.3]pCpNTA**) compared to previously reported **[3.3]pCp**-5,8,14,17-tetracarboxamide (**[3.3]pCpTA**). The **[n.n]pCpNTA** monomers also represent the reversal of a previously reported trend in solution-phase assembly strength when comparing **[2.2]pCpTA** and **[3.3]pCpTA** monomers. The origins of the assembly differences are geometric changes in the association between **[n.n]pCpNTA** monomers—revealed by computations and X-ray crystallography—resulting in a more favorable slipped stacking of the intermolecular π-surfaces (**[n.n]pCpNTA** vs. **[n.n]pCpTA**), and a more complementary H-bonding geometry (**[3.3]pCpNTA** vs. **[2.2]pCpNTA**).

Introduction

Supramolecular polymers (SPs) are a class of macromolecules formed by molecular self-assembly through reversible noncovalent interactions, resulting in polymeric properties in the bulk and in solution.[1] The size and strength of these intermolecular assemblies are determined by the equilibrium constant for monomer association K_a, or in the case of a bifunctional monomer, the elongation constant K_e, which is dependent on the nature of the noncovalent interaction, solvent composition, concentration, and temperature. Examples of noncovalent interactions utilized for SPs include hydrogen bonding, metal coordination, π-stacking, halogen bonding and hydrophobic interactions.[2] Altering the structural information encoded in the molecular recognition unit that comprises a supramolecular monomer enables tuning of the supramolecular assembly and ultimately the properties derived from these assemblies.[3]

The mechanism of supramolecular polymerization—isodesmic or cooperative—describes the monomer association constant K_a as a function of growing oligomer size.[4] The isodesmic mechanism is characterized by a single elongation constant K_e independent of assembly size.[5] The cooperative mechanism is characterized by two distinct association constants: the association constant between monomers in the molecularly dissolved state prior to the formation of a critical nucleus, is described by the nucleation constant (K_{nuc}), while a generally larger elongation constant (K_{elo}) describes association between monomers, the critical nucleus, and the growing polymer chain.[6] The mechanism and thermodynamics of supramolecular polymerization are highly sensitive to structural and electronic factors affecting both monomer and assembly.[7] By observing the individual influence of these structural and electronic factors on assembly mechanism and thermodynamics, information for the rational design of future supramolecular monomers can be achieved. These structure–property and structure–mechanism relationships have been performed for certain monomer classes,[7a] but fundamental differences between monomer classes necessitates establishing these relationships across a broad range of monomers to achieve a greater degree of generality and allow the rational design of new SPs.

In 2016, we reported a new SP monomer based on [2.2]paracyclophane-4,7,12,15-tetracarboxamide (**[2.2]pCpTA, Figure 1**).[8] These **[2.2]pCp** monomers self-assemble through intramolecular (transannular), and intermolecular hydrogen bonding to produce homochiral 1-D stacks composed of double-helical hydrogen bonding through *anti*- aligned amides, where the helical sense of the assembly is determined by the planar-chirality of the monomer. Further studies have assessed the role of transannular hydrogen bonding and its impact on assembly dynamics,[9] and computational support for the pathway selection and isodesmic supramolecular polymerization of the *anti*-conformer of **[2.2]pCpTA**.[10] This assembly mechanism is uncommon for hydrogen bond directed assemblies that normally feature cooperativity from strong H-bond polarization or dipole growth.[11]

Our previous work established a structure–property relationship in **[n.n]pCpTAs** by comparing **[2.2]pCpTA** to its bridge-expanded homolog [3.3]paracyclophane-5,8,14,17-tetracarboxamide (**[3.3]pCpTA**).[12] It was shown that while the

10.1002/chem.202003909

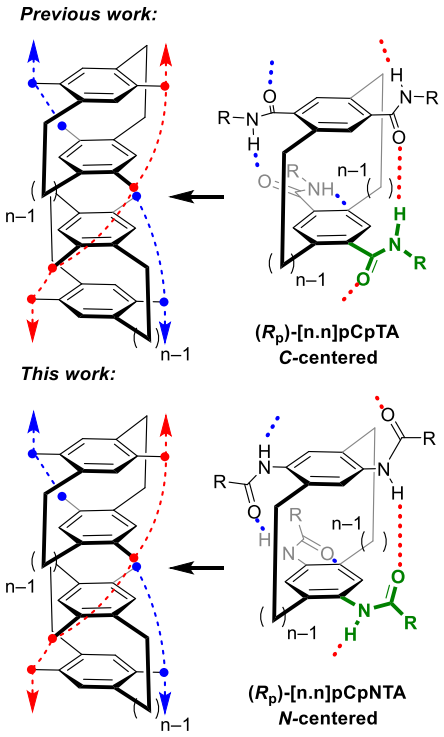

Figure 1. A representation of the hydrogen bond directed self-assembly of **[n.n]pCpTA** compared to **[n.n]pCpNTA**. Amide connectivity highlighted in green for emphasis.

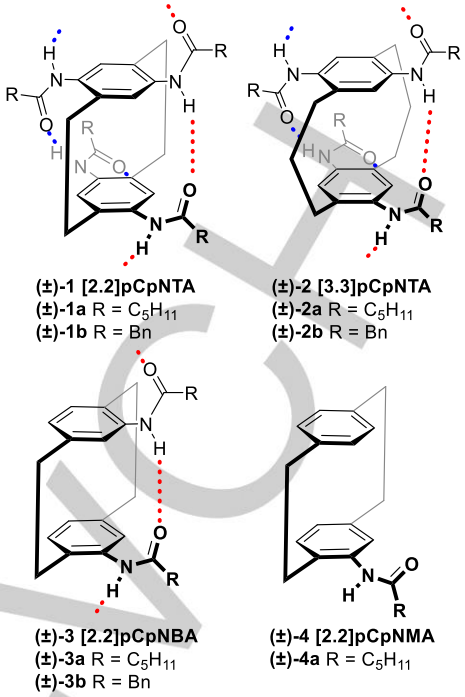

Figure 2. The **[n.n]pCp**-anilides studied in this work.

assembly geometry remained optimized, the additional carbon in the covalent bridge provided an increase in monomer entropy due to the scissoring action of the bridge *chair/boat* interconversion process. The results represent a flexibility–complementarity dichotomy[13] in SPs where the approximately equal complementarity in **[2.2]pCpTA** and **[3.3]pCpTA** assembly, but increased flexibility in **[3.3]pCpTA**, led to a weaker assembly.

We envision the **[n.n]pCpTA** scaffold to be particularly useful for developing structure–property relationships in SPs as the extensive preorganization of the monomer prevents significant structural changes upon intermolecular association, and so changes in assembly can be largely attributed to optimization of noncovalent interactions.

Previous studies of **[n.n]pCpTAs** were performed on amides with C_{ar}–C=O connectivity (*C*-amides or carboxamides). Analogous to various experiments done with the benzene trisamide (**BTA**) family of monomers,[14] our interest extended to different hydrogen bonding units, especially those featuring amides with C_{ar}–N–C=O connectivity (*N*-amides or anilides). A similar analysis of amide connectivity has been undertaken in the 1-D supramolecular polymerization of **BTA** derivatives, and C_3-symmetric oligo-phenylene ethynylene (**OPE**) derivatives.[15] In the case of **BTAs** it was found that the assembly of both amide derivatives was cooperative, with the anilides exhibiting a weaker, less cooperative assembly. In the **OPE** derivatives, the opposite was found. While both derivatives assemble cooperatively, the **OPE** anilides exhibited stronger assembly and greater cooperativity compared to the carboxamides. The uniquely rigid structural and conformational control of **[n.n]pCps** motivated us to examine the influence of amide connectivity and how it influences **[n.n]pCp** self-assembly (**Figure 1**).

Herein, we report the synthesis, transannular hydrogen bonding characterization, and self-assembly of new **[n.n]pCp** derivatives based on anilide hydrogen bonding. We present two monomers: the self-assembling "cross" **[2.2]pCp**-4,7,12,15-tetraanilide (**[2.2]pCpNTA (±)-1**) and **[3.3]pCp**-5,8,14,17-tetraanilide (**[3.3]pCpNTA (±)-2**), along with two comparator molecules: the pseudo-*ortho* **[2.2]pCp**-4,12-bisanilide (**[2.2]pCpNBA (±)-3**), and the mono- **[2.2]pCp**-4-anilide (**[2.2]pCpNMA (±)-4**). The self-assembling **[n.n]pCpNTA** systems are studied in solution and the solid state and related to the mono- **[2.2]pCpNMA** and pseudo-*ortho* **[2.2]pCpNBA** transannular H-bonding comparators in the absence of assembly. Alkyl chains (**(±)-1–4a**, R = C_5H_{11}) gave remarkable solubility in organic solvents for solution studies, while aromatic sidechains (**(±)-1–3b**, R = Bn) were chosen for single crystal X-ray diffraction studies (**Figure 2**).

Results and Discussion

Calculations

Molecular modelling and gas-phase DFT calculations of **[n.n]pCpTA** derivatives proved useful for examining amide conformations and how they relate to assembly structure and thermodynamics.[10] Geometry optimization of **[n.n]pCp**-anilides and previously studied **[n.n]pCpTA** monomers and dimers was performed at the ωB97X-D/6-31G level of theory rather than previously employed M06-2X/6-31G to better account for the influence of dispersion forces when studying noncovalent interactions (summarized in Tables S11–17).[16] The ground state of the **[n.n]pCp**-carboxamides feature amides that tilt out of the arene plane to relieve $A^{1,3}$ strain with the bridge hydrogens and either the carbonyl oxygen or secondary amide nitrogen. The

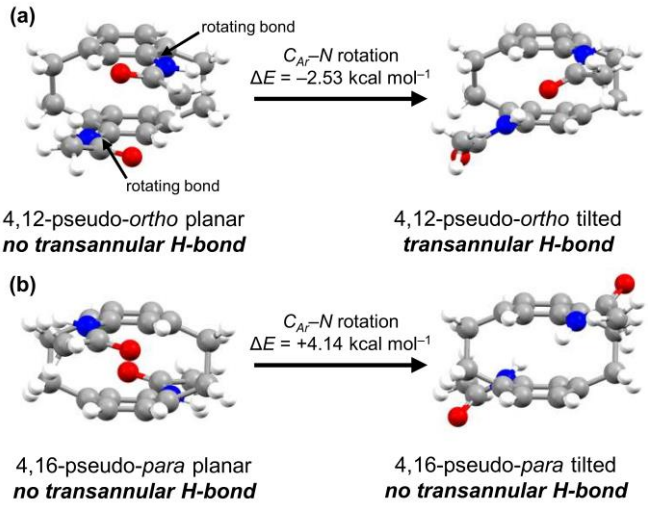

Figure 3. Thermodynamics of anilide conformers for simple 4,12-pseudo-ortho (a) and 4,16-pseudo-para **[2.2]pCp-**bisanilides from DFT calculations.

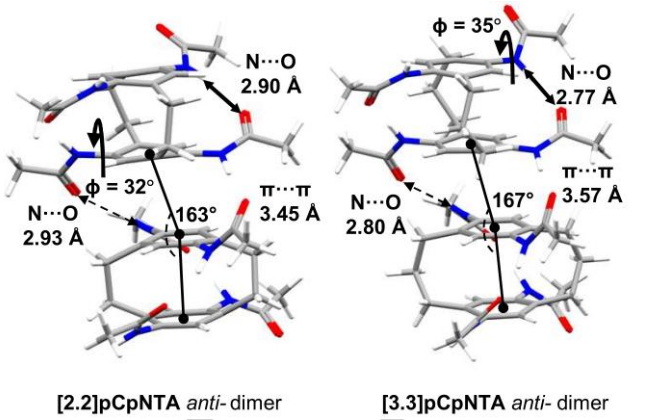

Figure 4. Optimized geometries of **[2.2]pCpNTA** and **[3.3]pCpNTA** *anti-* dimers from DFT calculations with important structural parameters highlighted.

anilides have less $A^{1,3}$ strain due to the smaller size of the N–H group, and therefore have a stable planar conformation. Calculations of the various **[n.n]pCp-**anilides reveals that in the absence of transannular hydrogen bonding, the anilide is *coplanar* with the aryl ring to maximize conjugation with the sp^2 hybridized nitrogen (see Table S14).

Simple **[2.2]pCp**-anilides are used to examine the energetic and geometric preferences for anilides in the presence and absence of transannular hydrogen bonding. **[2.2]pCp-**Monoanilides exhibit two local minima (Figure S56) corresponding to mostly coplanar (E_{rel} = 0 kcal mol^{-1}) and slightly tilted (E_{rel} = +1.9 kcal mol^{-1}) anilides. Pseudo-*ortho* positioned anilides—such as those in **(±)-3**, for example—can rotate out of the plane of the aromatic deck to optimize the geometry of transannular deck-to-deck hydrogen bonding (Figure S48).

When the anilides rotate out of plane of the aryl ring to participate in transannular hydrogen bonding, the pseudo-*ortho* bisanilide gains back the enthalpic stabilization it loses from the loss of conjugation between the aryl deck and the sp^2 hybridized nitrogen plus the free energy gain from an anilide hydrogen bond (ΔE = –2.5 kcal mol^{-1}, Figure 3a). The hydrogen bonding stabilization does not occur in the pseudo-*para* derivative, making its anilide tilting unfavorable (ΔE = +4.1 kcal mol^{-1}, Figure 3b). Comparing the tilted (H-bonded) conformer of 4,12-pseudo-*ortho* **[2.2]pCp-**bisanilide with the tilted conformer of 4,16-pseudo-*para* **[2.2]pCp-**bisanilide can reveal the strength of transannular H-bonding (9.6 kcal mol^{-1})—nearly the same as that observed when comparing the analogous **[2.2]pCp-**biscarboxamides (10.5 kcal mol^{-1}).

Similar to **[2.2]pCpTA**, there are two low energy conformers of **[2.2]pCpNTA**, depicted in Figure S50. The *syn-* (E_{rel} = +0.32 kcal mol^{-1}) and the *anti-* (E_{rel} = 0 kcal mol^{-1}) conformers differ in H-bonding directionality with respect to the assembly axis. The relative stability of the *anti-* conformer holds true for the **[3.3]pCpNTA** series as well, with the *syn-* conformer disfavored by 2.2 kcal mol^{-1}. Especially important is the anilide conformation with respect to the C_5–C_4–N–C(=O) dihedral angle, which we have previously shown to be intimately linked to the intermolecular π···π distance.[12] In this case, the dihedral angles in **[2.2]pCpNTA** (32.7°, –141.7°, *anti-* conformer) are slightly smaller than those observed for **[2.2]pCpTA** (39.6°, –147.3°, *anti-*conformer), indicating the intermolecular π···π distance could be slightly closer than that of the **[2.2]pCpTAs** upon optimization of intermolecular hydrogen bonding. The extension of the paracyclophane bridge by one carbon also increases the torsion of the anilides to maintain optimum transannular hydrogen bonding in the **[3.3]pCpNTA** derivatives, and further in the **[3.3]pCpTA** derivatives.

Comparison of the computed structures and energies of both *syn-* and *anti-* **[n.n]pCpNTA** dimers reveals the thermodynamic favorability for assembly of the *anti-* conformer (*syn* = + 11.9 kcal mol^{-1} for **[2.2]pCpNTA**, *syn* = + 16.8 kcal mol^{-1} for **[3.3]pCpNTA**), consistent with what was observed in prior work for **[2.2]pCpTA** and **[3.3]pCpTA**.[8, 10, 12] Extrapolation of the computational results of **[2.2]pCpTA**[10] indicate that, if anilide rotation (about the C_{ar}–N bond) still maintains a low barrier, the assembly of **[n.n]pCpNTAs** likely occurs through pathway selection of the *anti-* conformer and adheres to an isodesmic mechanism.[10]

Interestingly, the computed gas-phase interaction energies—obtained from the difference in energy of a geometry optimized dimer compared to two isolated monomers—reveals a 4.3 kcal mol^{-1} larger interaction energy for **[2.2]pCpNTA** *anti-* compared to **[2.2]pCpTA** *anti-* (–46.2 kcal mol^{-1} for **[2.2]pCpNTA** compared to –41.9 kcal mol^{-1} for **[2.2]pCpTA**). The *syn-* conformers have > 7 kcal mol^{-1} less binding energy than the *anti-* conformers (summarized in Table S15). Similarly, the **[3.3]pCpNTA** *anti-*dimer (–50.3 kcal mol^{-1}) has a 7.2 kcal mol^{-1} larger interaction energy than the **[3.3]pCpTA** *anti-* dimer (–43.1 kcal mol^{-1}, summarized in Table S17). The interaction energy for **[3.3]pCpNTA** is ca. 4 kcal mol^{-1} larger than that of **[2.2]pCpNTA**. The reasons become clear when the dimer geometries are examined, with the **[2.2]pCpNTA** dimer featuring longer H-bonding distances and shorter π···π distances (Figure 4) which should contribute to a weaker binding enthalpy. Although the gas phase estimation of interaction energy is an oversimplification of a dynamic solution environment, it indicates the potential for stronger assembly of **[n.n]pCpNTAs** compared to **[n.n]pCpTAs**, as well as stronger assembly of **[3.3]pCpNTA** compared to **[2.2]pCpNTA**.

Synthesis

10.1002/chem.202003909

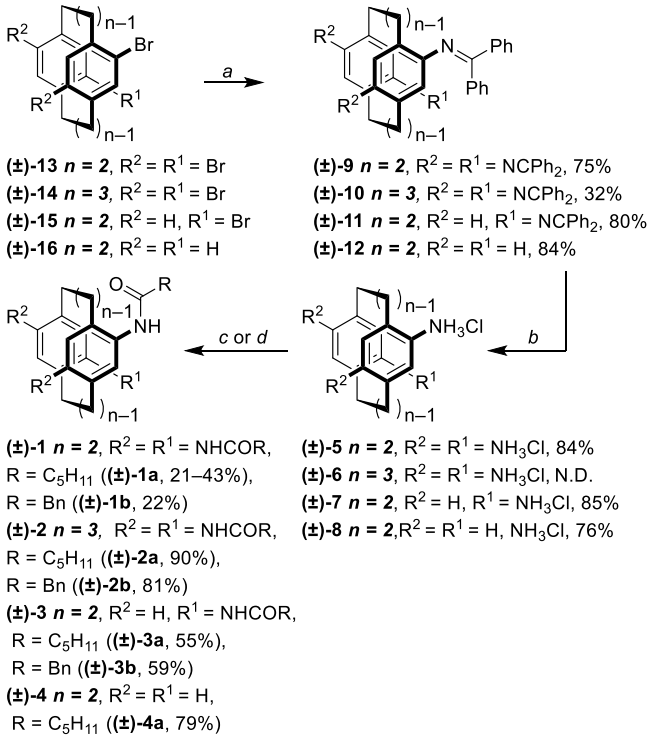

Scheme 1. The synthesis of **[n.n]pCp**-anilide target molecules **(±)-1–4a** and **(±)-1–3b**. Reagents: *a* Pd(dppf)Cl_2 (5–20 mol%), benzophenone imine (2.5 equiv/Br), NaO*t*Bu (1.5 equiv/Br), toluene, 110 °C, 48 h; *b* HCl (conc.), THF, rt, 8 h; *c* THF, NEt_3, RCOCl, rt, 12 h; *d* NaOH, RCOCl, toluene rt, 12 h. Yields for **(±)-7** and **(±)-8** reported as amines after aq. NaOH wash and extraction with DCM.

Surprisingly, until now, only one example of a **[2.2]pCp** with four nitrogen substituents directly bound to the **[2.2]pCp** ring system (all benzophenone imines) has been reported.[17] Unlike other examples in that work, the 4,7,12,15-**[2.2]pCp**-tetra(benzhydrilideneimine) was not hydrolyzed to the free tetraamine (conc. HCl in THF, then NaOH), presumably, and later confirmed by our work, because of the instability of this incredibly electron rich aromatic amine complicating isolation and characterization. We imagined this crucial 4,7,12,15-**[2.2]pCp**-tetraamine could come from the known intermediate 4,7,12,15-**[2.2]pCp**-tetra(benzhydrilideneimine), and upon hydrolysis and acylation, promote the synthesis of **[2.2]pCpNTA**. The comparator **[2.2]pCpNBA** and **[2.2]pCpNMA** could come from the corresponding known monoamines by simple acylation chemistry. Upon optimization of the synthesis of **[2.2]pCpNTA** beginning with commercially available **[2.2]pCp**, we envisioned adapting the same procedures to the **[3.3]pCp** system starting from previously prepared "crossed" 5,8,14,17-**[3.3]pCp**-tetrabromide.[12]

The synthesis of *N*-substituted **[2.2]pCps** (Scheme 1) began from the corresponding **[2.2]pCp** bromides,[18] which underwent Buchwald–Hartwig coupling with the ammonia equivalent benzophenone imine under palladium catalysis.[17] Imino **[2.2]pCps** could be hydrolyzed to the corresponding ammonium salts with HCl in THF. Deprotonation to the free amine was accompanied by instant decomposition in **(±)-5** and slower decomposition of **(±)-7** and **(±)-8** in solution accompanied by the formation of a deep blue-green color. Therefore, deprotonation of the ammonium salts and reaction with an appropriate electrophile was performed in the same flask to minimize decomposition.

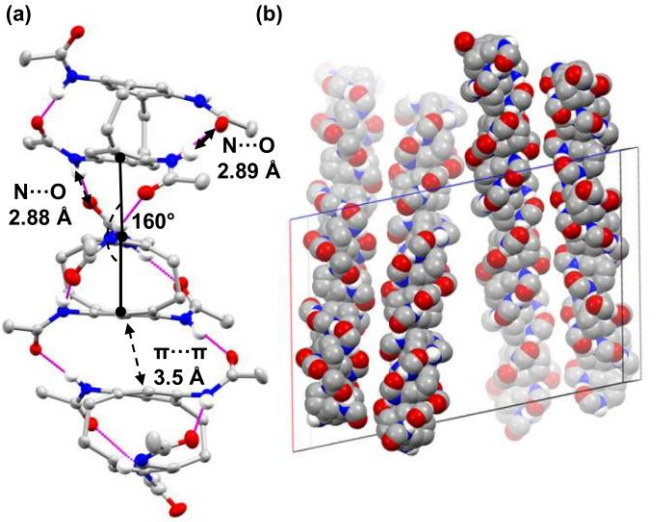

Figure 5. Trimer of **(R_p)-1b** obtained from single crystal X-ray diffraction with average distances highlighted (a). Hydrogen bonds shown in magenta. Crystal packing of columnar homochiral stacks in the unit cell of **(±)-1b** viewed as a space filling model (b). Hydrogen atoms not involved in hydrogen bonding, disorder, solvent molecules, and benzyl sidechains omitted for clarity. Ellipsoids in (a) shown at the 50% probability level. Atom color code: O red, N blue, C gray, H white.

Acylation of the amino-**[n.n]pCps** with hexanoyl chloride gave *n*-pentyl substituted anilides **(±)-1–4a** suitable for solution studies, while phenylacetyl chloride was used to give benzyl anilides **(±)-1–3b** for study by single crystal X-ray diffraction. For the final acylation, either NEt_3 in THF or Schotten–Baumann reaction conditions (toluene and aq. NaOH) worked equally well. Once the synthesis of **[2.2]pCpNTA** was completed and optimized, the approach was easily extended to the **[3.3]pCpNTA** system beginning with the synthesis of **(±)-10** under identical conditions as **(±)-9**. Best results were obtained for the synthesis of **(±)-1a** and **(±)-2a** by performing hydrolysis and acylation in the same reaction vessel, as isolation of the ammonium salts proved troublesome, and was accompanied by decomposition. Overall yields for the synthesis of target molecules **(±)-1a** (27%) and **(±)-2a** (29%) from the corresponding tetrabromides **(±)-13** and **(±)-14** were quite reasonable.

Worth noting is the outstanding solubility of **(±)-1–3a** in nonpolar solvents such as methylcyclohexane. Concentrated solutions of **(±)-1a** (up to 50 mM in MCH) could be prepared and were soluble for weeks. Similarly concentrated solutions of **[2.2]pCpTA** with *n*-hexyl sidechains would precipitate after ~1 day. Even **(±)-4a**, with only one H-bonding unit and no intramolecular H-bonding, could not be dissolved in MCH at room temperature.

X-ray crystallography

Crystals of **(±)-1a** were composed of tightly bundled needle-like fibers, so an aromatic benzyl sidechain was introduced to **(±)-1b** to aid in single-crystal growth. Single crystals of suitable quality for X-ray diffraction were grown by slow evaporation from an EtOAc/EtOH solution.

The infinitely extended self-complementary SP structure of **(±)-1b** is observed in the crystal, giving insight into structural

factors that likely govern solution-phase SP formation. Selected average interatomic distances for the X-ray structure of **(±)-1b** are shown in Figure 5a. All the molecules of **1b** are engaged in intermolecular hydrogen bonding to neighboring **1b** molecules through *anti*- aligned anilides, with slightly longer H-bonds than in **[2.2]pCpTA** (average N···O distance 2.88 Å for **1b** compared to 2.84 Å for **[2.2]pCpTA**).[8] Every fourth repeat unit, one H_2O molecule provides one H-bond donor and acceptor between anilides of **(±)-1b**. Remarkably, the intermolecular π···π distances (centroid···centroid) in the X-ray structure of **(±)-1b** are much closer than those of the *C*-centered derivative (average distance of 3.5 Å for **(±)-1b** compared to 3.8 Å for **[2.2]pCpTA**). This closer π···π distance is accompanied by a slight slippage of the π-surface between **(±)-1b** monomers (centroid···centroid···centroid angle of 160° compared to 172° in **[2.2]pCpTA**). It is well accepted that the sandwich-type stacking of benzene rings is the least favorable arrangement, and that the interaction energy of the benzene dimer increases as the parallel stacks increase their displacement.[19] Therefore, the slight slippage of the intermolecular π-decks can lead to a decrease in repulsive π···π interactions compared to **[2.2]pCpTA**, while still optimizing intermolecular and transannular H-bonding.

The unit cell of **(±)-1b** is vast (nearly 25,000 Å^3), containing 24 molecules of **(±)-1b** as well as several EtOH and H_2O solvent molecules positioned between the stacks. This unit cell is composed of eight individual homochiral assemblies. These assemblies can be further divided in half along the *c*-axis to give two sets of four (two R_p, two S_p) stacks. Each of the four stacks extends in parallel to the others in the set, and at an angle of approximately 25° to the other set of four stacks (Figure 5b, see also Figure S39).

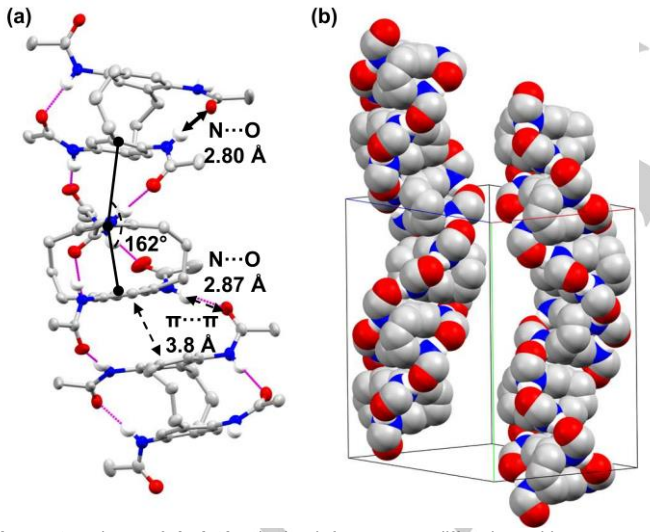

Figure 6. Trimer of **(R_p)-2b** obtained from X-ray diffraction with average distances highlighted (a). Hydrogen bonds shown in magenta. Crystal packing of **(±)-2b** featuring homochiral hexamers extending beyond the unit cell (b). Hydrogen atoms not involved in hydrogen bonding, solvent molecules, disorder, and benzyl sidechains omitted for clarity. Ellipsoids in (a) shown at the 50% probability level. Atom color code: O red, N blue, C gray, H white.

Crystals of **(±)-2a** exhibited the same needle-like morphology as **(±)-1b**, necessitating the introduction of benzyl sidechains in **(±)-2b**. Single crystals of **(±)-2b** sufficient for X-ray diffraction were grown by slow evaporation of a 1,4-dioxane solution. Similar to **(±)-1b**, **(±)-2b** in the crystal displays the 1-D columnar structure of its self-complementary SP. The unit cell of **(±)-2b** features a pair of enantiomeric homochiral tetramers stitched together by double helical *anti*- aligned anilide hydrogen bonding with the benzyl sidechains, and 1,4-dioxane solvent molecules, filling the space between individual stacks. Consistent with our previous crystal structure of **[3.3]pCpTA**, the central bridge carbon is disordered, representing a likely combination of *chair* and *boat* bridge conformers.[12, 20]

Although the intermolecular N···O distance in **(±)-2b** (2.87 Å) is nearly identical to **(±)-1b**, the average transannular N···O distance in **(±)-2b** (2.80 Å) is considerably shorter as the anilides in **(±)-2b** rotate further out of the aryl plane in order to optimize transannular hydrogen bonding across a longer deck-to-deck distance (Figure 6a). The consequence is two anilides that rotate nearly orthogonal to the aryl plane (θ = 87.3°, 72.8°). These extremely tilted anilides are accompanied by anilides with shallower dihedral angles (ca. 30–40°) to give the assembly a distinct "major and minor groove" (Figure 6b). The large range of anilide dihedral angles (28–87°) is a simultaneous result of the increased deck-to-deck distance, and the increased $A^{1,3}$ strain encountered with aryl substituents in the 5-position of the **[3.3]pCp** skeleton. When the monomer is placed in a dynamic solution-phase environment, all anilide, and bridge conformations, are likely represented.

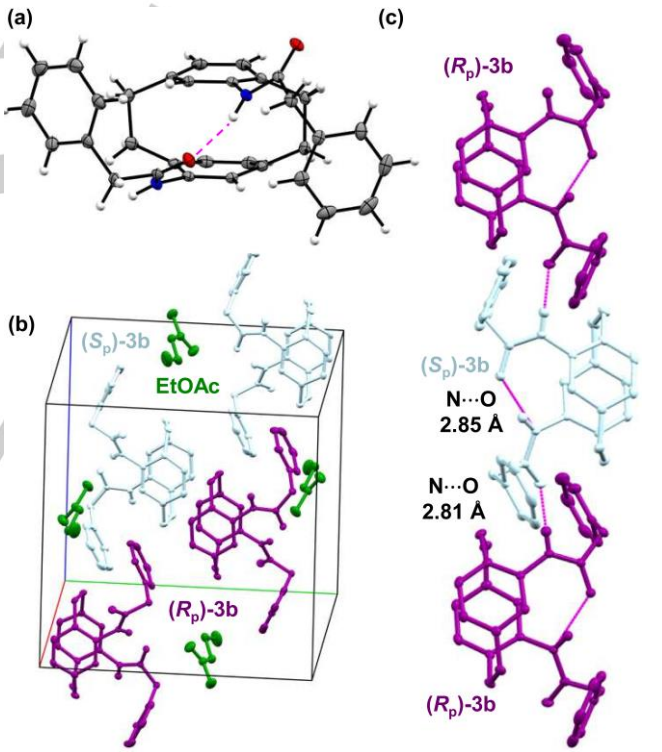

Figure 7. ORTEP plot of **(R_p)-3b** at the 50% probability level from X-ray diffraction with transannular hydrogen bond shown as magenta dashed line (a). Atom color code: O red, N blue, C gray, H white. Unit cell of **(±)-3b** with **(S_p)-3b** shown in light blue, **(R_p)-3b** shown in purple, and ethyl acetate shown in green (b). Hydrogen bonding propagation alternating between transannular H-bond and intermolecular H-bond between **(S_p)-3b** and **(R_p)-3b**. H-bonds shown in magenta.

To further examine the transannular hydrogen bonding between pseudo-*ortho* (i.e., 4,12-substituted) anilides present in **(±)-1–3** without the influence of the second pair of anilides (i.e., 7,15-substituted), single crystals of the transannular H-bond comparator **(±)-3b** were grown by slow evaporation of an

10.1002/chem.202003909

EtOH/EtOAc solution. The transannular H-bond is maintained (Figure 7a, N···O distance = 2.85 Å) and is slightly shorter than that in pseudo-*ortho* **[2.2]pCp-**biscarboxamide (N···O distance = 2.90 Å).[9] The unit cell of **(±)-3b** features four molecules of **3b** (two of **(R_p)-3b** and two of **(S_p)-3b**) and four EtOAc solvent molecules (Figure 7b). In contrast to pseudo-*ortho* **[2.2]pCp-**bisamide, which formed intermolecular H-bonds with MeOH solvent molecules, **3b** forms self-complementary anilide hydrogen bonds (N–H···O) between molecules of opposite configuration (Figure 7c, N···O distance 2.81 Å). The heterochiral association of **(±)-3b** in the solid state is an example of the three-point contact rule for homochirality,[21] and confirms the necessity of a second intermolecular interaction to instruct stereospecific self-assembly like that observed in **(±)-1b** and **(±)-2b**.

It should be noted that the X-ray crystallographic data obtained for compounds **(±)-1–3b** with aromatic sidechains is expected to be different than that of compounds **(±)-1–3a** with aliphatic sidechains. Care should be taken when comparing data between related compounds where sidechain packing influences the crystal structure, but in the absence of suitable crystals for **(±)-1–3a**, analysis of **(±)-1–3b** represents the best approximation of assembly structure.

Solution studies

Solution-phase assembly characterization of **[n.n]pCp-**anilides **(±)-1–4a** was carried out using ^{1}H NMR and FT-IR spectroscopy. In the assembled state, **(±)-1a** possesses two non-equivalent anilide N–Hs corresponding to transannularly H-bonded H_a and intermolecularly H-bonded H_b as well as two non-equivalent aromatic C–Hs corresponding to hydrogens *ortho* to each respective anilide (H_c, H_d, Figure 8a). In moderately polar solvents like $CDCl_3$, anilide rotation is fast on the NMR timescale, and the anilide N–H resonances represent a time average of the transannularly H-bonded, intermolecularly H-bonded, and solvent exposed environments. The chemical shift of the N–H resonance in transannular H-bond comparator **(±)-3a** can be used as a reference for a molecularly dissolved **(±)-1a**, lacking intermolecular H-bonding since its association constant in $CDCl_3$ was shown to be negligible from 0.1–30 mM (Figure S5). An increase in concentration of **(±)-1a** (R = C_5H_{11}) in $CDCl_3$ results in a deshielding of the anilide N–H resonance and a shielding of the aromatic C–H resonance due to an increase in H-bonding and π-stacking, respectively (Figure 8b). This trend is similar to what is observed in the previously reported **[n.n]pCpTAs**.[8] The concentration change (0.025 mM to 30 mM) sees the chemical shift of the anilide N–H move from near molecularly dissolved at 8.13 ppm towards aggregated at 8.91 ppm ($\Delta\delta$ = 0.78 ppm). For reference, the chemical shift of **(±)-3a** varies between 8.18 and 8.07 ppm ($\Delta\delta$ = 0.11 ppm) from 30–0.1 mM indicating very weak intermolecular association. Fitting the change in the anilide N–H chemical shift of **(±)-1a** to an isodesmic model gives an elongation constant (K_e) of 2175 ± 90 M^{-1} (Figure 8c),[1] over 30-fold higher than that observed for the *C*-centered isomer (K_e = 64 ± 5 M^{-1}). Despite the same number of intermolecular H-bonds, the assembly of **(±)-1a** is more thermodynamically favorable than that of **[2.2]pCpTA** under the same conditions ($\Delta\Delta G°$ = –2.1 kcal mol^{-1}). The isodesmic mechanism is consistent with analogous self-assembling **[n.n]pCps**[8, 10, 12] and is likely a result of pathway selection of the *anti*- conformer.

The stronger assembly of **(±)-1a** compared to **[2.2]pCpTA** is also confirmed by cooling a solution of **(±)-1a** (10 mM) in $CDCl_3$. As the solution is cooled, the anilide N–H (H_a and H_b) and aromatic C–H (H_c and H_d) resonances decoalesce when anilide rotation slows on the NMR timescale (Figure 8d). The resolution of these individual resonances is caused by intermolecular H-bonding between associated monomers of **(±)-1a** raising the barrier for anilide rotation, since rotating the anilides in an elongated assembly would require breaking consecutive intermolecular and transannular H-bonds. For comparison, the

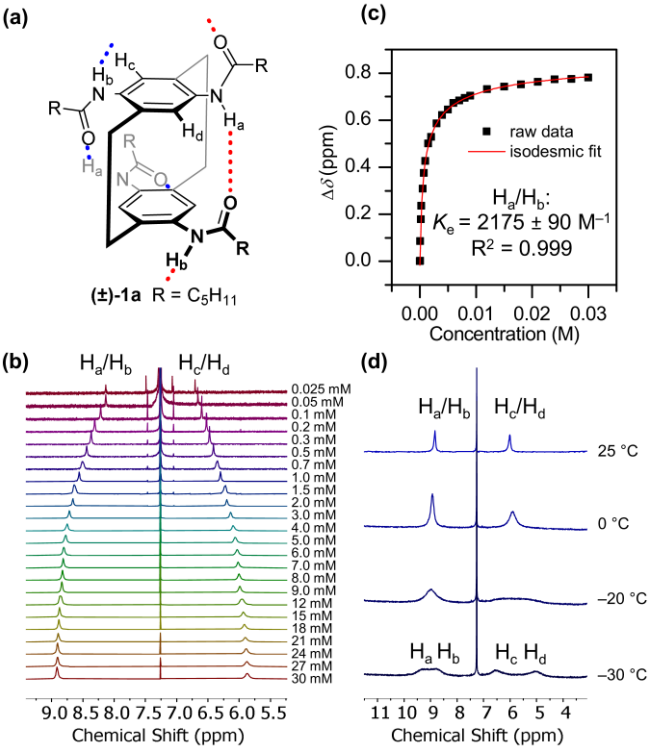

Figure 8. Assignments of ^{1}H NMR chemical shifts for **(±)-1a** in the assembled state (a). Variable concentration (0.025–30 mM) ^{1}H NMR of **(±)-1a** in $CDCl_3$ (b) and fitting of the concentration-dependent change in anilide N–H chemical shift to an isodesmic model (c). Low temperature (25 to –30 °C) ^{1}H NMR of **(±)-1a** (10 mM) in $CDCl_3$ (d).

amide N–H and aromatic C–H resonances of **[2.2]pCpTA** in $CDCl_3$ remain coalesced down to the same temperatures, indicating stronger assembly in **(±)-1a**.[8] Solutions of **(±)-3a** exhibit only one anilide N–H resonance down to –50 °C (Figure S14), confirming the change is a result of intermolecular assembly. Analogous to **(±)-1a**, compound **(±)-2a** in the assembled state possesses two non-equivalent anilide N–Hs ($H_{a'}$ and $H_{b'}$) and two non-equivalent aromatic C–Hs ($H_{c'}$ and $H_{d'}$) if *chair/boat* interconversion and anilide rotation remain fast on the NMR timescale (Figure 9a). Variable concentration NMR of **(±)-2a** shows an identical trend to **(±)-1a** as the anilide resonance $H_{a'}/H_{b'}$ becomes deshielded upon an increase in concentration due to hydrogen bonding (8.25 ppm at 0.025 mM to 9.20 ppm at 30 mM, $\Delta\delta$ = 0.95 ppm) and the aromatic C–H resonance $H_{c'}/H_{d'}$ becomes shielded (6.84 ppm at 0.025 mM to 6.10 ppm at 30 mM) due to π-

[1] Uncertainty of data fitting reported. Error estimated as ± 15 %.

10.1002/chem.202003909

stacking (Figure 9b). Fitting the change in chemical shift of $H_{a'}/H_{b'}$ for **(±)-2a** in $CDCl_3$ to an isodesmic model gives an elongation constant (K_e) of 5303 ± 277 M^{-1} (Figure 9c), indicating a thermodynamically more stable assembly for **(±)-2a** compared to **(±)-1a**. The assembly of **(±)-2a** compared to *C*-centered **[3.3]pCpTA** is **~300-fold stronger** based on comparison of K_e (17 M^{-1} for **[3.3]pCpTA** in $CDCl_3$). The chemical shift of the N–H resonance in the assembled state of **(±)-2a** (9.20 ppm) is slightly deshielded compared to that in **(±)-1a** (8.91 ppm) indicating the hydrogen bonding geometry of **(±)-2a** could be slightly more favorable as observed in DFT calculations of the **[n.n]pCpNTA** dimers.

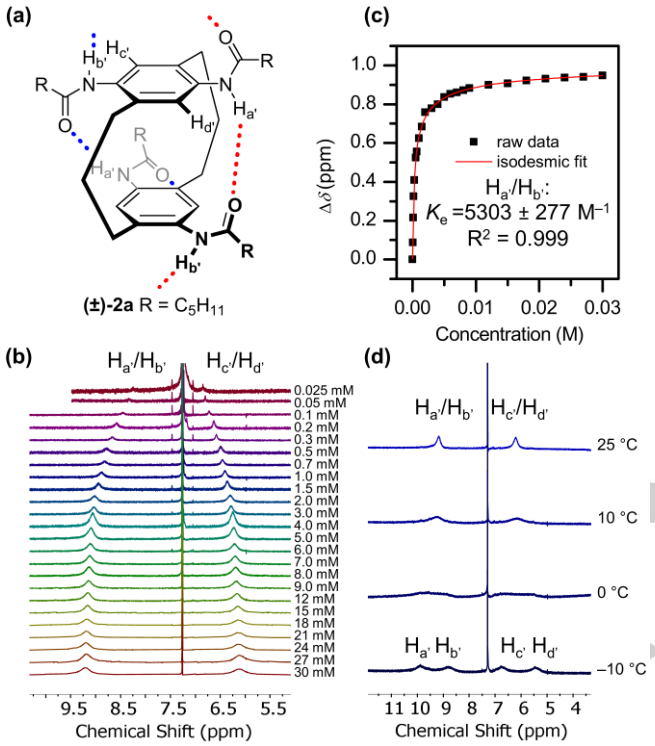

Figure 9. Assignments of the chemical shifts of **(±)-2a** in the assembled state if *chair/boat* interconversion remains time averaged (a). Variable concentration (0.025–30 mM) ^{1}H NMR of **(±)-2a** in $CDCl_3$ at 298 K (b). Fitting of the NMR data from (b) to an isodesmic model (c). Variable temperature ^{1}H NMR of **(±)-2a** 10 mM in $CDCl_3$ (d).

Further evidence for the stronger assembly of **(±)-2a** compared to **(±)-1a** comes by cooling a 10 mM solution of **(±)-2a** in $CDCl_3$. The same decoalescence due to slow anilide rotation in **(±)-1a** at –20 °C was observed at 0 °C for **(±)-2a**, indicating stronger intermolecular assembly at higher temperatures (Figure **9** 9d). DOSY NMR was used to confirm concentration-dependent polymeric assemblies of **(±)-1a** and **(±)-2a** that were larger than those of the corresponding **[n.n]pCpTAs** under identical conditions in $CDCl_3$, although the diffusion coefficients for **(±)-1a** and **(±)-2a** were nearly identical and could not confirm larger polymeric structures for **(±)-2a** compared to **(±)-1a** (Table S3–4). When **(±)-1a** and **(±)-2a** are dissolved in cyclohexane or methylcyclohexane (MCH)—nonpolar, assembly favorable solvents—the solutions exhibit the viscosity of honey at millimolar concentrations, a hallmark feature of SPs. Intermolecular assembly is evidenced for **(±)-1a** by ^{1}H NMR in cyclohexane-d_{12}, where persistent H-bonding causes broadening of all resonances and resolution of the four individual anilide N–H (H_a and H_b) and aromatic C–H resonances (H_c and H_d) expected in the assembled state. Assembly of **(±)-1a** in cyclohexane-d_{12} is maintained even at low concentrations (0.1 mM) and high temperatures (70 °C, see Figure S10), further evidence that the assembly of **(±)-1a** is stronger than that of **[2.2]pCpTA**, which disassembles when heated in cyclohexane-d_{12}. Additionally, it was found that adding a small volume fraction of $CDCl_3$ to the cyclohexane-d_{12} solution could break up the polymeric structures of **(±)-1a** (Figure S11).

Assembly state can be confirmed by examining the characteristic H-bonding energies of the C=O and N–H stretches with IR spectroscopy (Figure 10, summarized in Table S7).

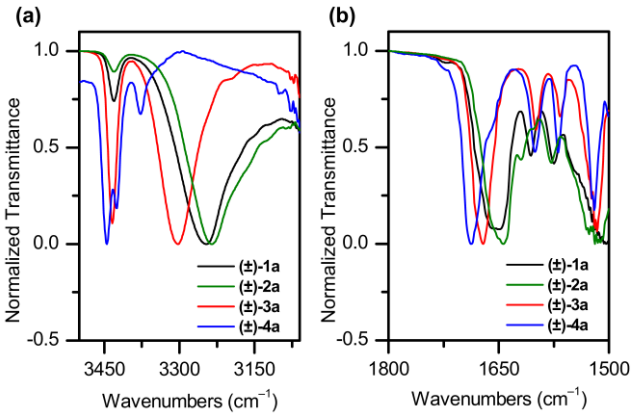

Figure 10. Overlaid and normalized FT-IR spectra of the N–H (a) and C=O (b) regions of **(±)-1–4a** 10 mM in $CHCl_3$ and MCH.

Solutions of **[2.2]pCp**-anilides **(±)-1–4a** in solvents like chloroform, which favor the molecularly dissolved state,exhibit a solvent exposed N–H (~3430 cm^{-1}) and a broad, H-bonded N–H (comprised of overlapping intermolecularly and transannularly H-bonded N–Hs) that moves to lower energy with increasing concentration (3303–3244 cm^{-1}).[9] Solutions of monoanilide **(±)-4a** in chloroform feature only a solvent exposed N–H (3445, 3425 cm^{-1}), while positioning of a second anilide in the pseudo-*ortho* position facilitates transannular H-bonding, and a second, H-bonded N–H appears (3303 cm^{-1}). The intermolecular assembly of **(±)-1a** in chloroform, as evidenced by ^{1}H NMR, is confirmed by the shift of the H-bonded N–H to lower energy (3264 cm^{-1} at 1 mM to 3244 cm^{-1} at 30 mM). The H-bonded N–H in **(±)-2a** follows the trend observed in **(±)-1a** but its peak appears at lower energy (3234 cm^{-1}) at the same concentration, again indicating the slight geometric preference for H-bonding in **(±)-2a**.

Similarly, the C=O signal of **[n.n]pCp**-anilides **(±)-1–4a** is sensitive to transannular H-bonding and intermolecular assembly. The peak corresponding to the C=O stretch in $CHCl_3$ moves from 1687 cm^{-1} in molecularly dissolved **(±)-4a** to 1671 cm^{-1} in transannular H-bonding **(±)-3a**, to 1658 cm^{-1} and 1644 cm^{-1} in assembling **(±)-1a** and **(±)-2a**, respectively.

When **(±)-3a** is dissolved in MCH, it is capable of weak intermolecular association, evidenced by the decrease in intensity of the solvent exposed N–H and shift of the H-bonded N–H to lower energy (3258 cm^{-1}). Similarly, **(±)-1a** and **(±)-2a** in MCH are exclusively in the assembled state and show a single, broad H-bonded N–H (3239 cm^{-1} in **(±)-1a**, 3226 cm^{-1} in **(±)-2a**) and no solvent exposed N–H, indicating high degrees of polymerization and lack of appreciable end groups, consistent with what has been observed in other self-assembling **[n.n]pCps**. This N–H

signal is independent of concentration (from 1–30 mM), consistent with what is observed by ^{1}H NMR, and occurs at the same energy as the solid-state N–H where all H-bonds are satisfied.

Evaluation of the thermodynamics of assembly for SPs in dilute nonpolar solution can be done with UV-vis spectroscopy. The strength of the assembly of **(±)-1a** in nonpolar solvents such as cyclohexane or MCH as evidenced by ^{1}H NMR indicates that the assembly should be persistent at micromolar concentrations used for UV-vis, even at high temperatures. This is confirmed by UV-vis spectroscopy where variable temperature UV-vis of **(±)-1a** and **(±)-2a** (10 μM in MCH) revealed no clear isosbestic points (Figure S30), supporting the predominance of the assembled state at these concentrations and temperatures. Attempts to break up the assemblies with the addition of $CHCl_3$ resulted in the major absorbance overlapping with the absorbance of $CHCl_3$ (Figure S31).

The results of our previous studies[9] indicate that circular dichroism spectroscopy of resolved amido **[2.2]pCps** have strong absorbances up to 350 nm. We believe that optical resolution will allow evaluation of assembly thermodynamics in dilute solution with CD spectroscopy using the appropriate solvent polarity/concentration combination. These studies are currently underway.

Conclusions

We have presented SPs based on **[n.n]pCp-**anilides (n = 2,3) as a way to examine the influence of amide connectivity on the supramolecular polymerization of **[n.n]pCps**. The change of amide connectivity from previously studied *C*-centered carboxamides to *N*-centered anilides led to a significant increase in K_e for monomers **(±)-1** and **(±)-2** in chloroform. The connectivity change is also accompanied by changes in anilide conformation which were explored through computations and by the synthesis of non-assembling comparators **(±)-3** and **(±)-4**. The transannular anilide H-bond is maintained in the pseudo-*ortho* derivative **(±)-3** in solution and in the solid state, while anilide rotation remains fast on the assembly timescale.

Underpinning the H-bond directed assembly of **[n.n]pCpNTAs** is a balancing act between enthalpically favorable formation of hydrogen bonds and enthalpically unfavorable face-to-face benzene stacking. Based on computational results, X-ray crystallographic evidence, and solution studies, the stronger solution-phase assembly of **(±)-1** and **(±)-2** compared to their *C*-centered **[n.n]pCpTA** counterparts can be attributed to subtle changes in intermolecular geometry. In the assembly of **(±)-1**, for example, despite average longer H-bonding distances and closer π···π distances—which should result in a weaker assembly—the slipped stacking of the aryl rings reduces the enthalpic penalty associated with a repulsive sandwich π–π interaction, leading to a net larger binding energy. The same trend is apparent in **(±)-2** where larger anilide dihedral angles lead to a longer π···π distance and allow further optimization of intermolecular H-bonds. The flexibility–complementarity dichotomy[13] can be invoked to assess differences in assembly strength in the **[n.n]pCp** derivatives.

In our previous report,[12] the similar hydrogen bonding complementarity between **[2.2]pCpTA** and **[3.3]pCpTA** but an increase in flexibility for **[3.3]pCpTA** led to a weaker assembly. For **[n.n]pCpNTAs**, the opposite trend is observed. The **[3.3]pCpNTA** assembly has increased flexibility, but now is accompanied by a more complementary binding geometry. This increased complementarity overrides the flexibility, leading to overall stronger supramolecular assembly. The supramolecular polymerization of the tetraanilides **(±)-1a** and **(±)-2a** in solution adhere to an isodesmic mechanism likely through pathway selection of the *anti*- conformer,[10] with a K_e in $CDCl_3$ that is 30–300-fold larger than their *C*-centered analogs despite the same number of intermolecular hydrogen bonds. Crystal structures of **(±)-1b** and **(±)-2b** reveal their preference for homochiral assemblies in the solid state while heterochiral interactions in **(±)-3b** confirm the need for a second H-bond to maintain homochiral assembly.

The difference in solution-phase assembly thermodynamics is attributed to the preferred slipped stack orientation of monomers in **(±)-1** and **(±)-2**, and the more complementary H-bonding geometry in **(±)-2** compared to **(±)-1** revealed by computations, and confirmed by X-ray crystallography, NMR, and IR spectroscopy.

This work demonstrates the large influence that seemingly small structural changes can have on supramolecular assembly, and highlights the utility that **[n.n]pCps** play as model systems for controlling SP structure, stereochemistry, mechanism, and thermodynamics. Until now, efforts to determine the influence of amide connectivity on 1-D SPs have focused on systems that self-assemble by cooperative mechanisms. The structural definition of **[n.n]pCps** allows for the control of H-bond polarization through transannular hydrogen bonding. The result is an isodesmic assembly regardless of hydrogen bonding unit, with the difference between assembly thermodynamics attributed solely to differences in noncovalent binding.

Experimental Section

For experimental details, see the Supporting Information.

Acknowledgements

Acknowledgement is made to the Donors of the *American Chemical Society Petroleum Research Fund* (PRF #56665-ND4) and to the National Science Foundation (CHE-1904534) for funding support of this research. K.A.A. wishes to acknowledge the NSF and the University of Florida for funding of the X-ray diffractometer through grant CHE-1828064. We acknowledge University of Florida (UF) Research Computing for providing computational resources and support that have contributed to the research results reported in this publication (https://www.rc.ufl.edu). The mass spectrometric data were obtained by the UF Department of Chemistry Mass Spectrometry Research and Education Center supported, in part, by the National Institutes of Health (NIH S10 OD021758-01A1). We would also like to thank Ion Ghiviriga and the UF Center for Nuclear Magnetic Resonance Spectroscopy for providing equipment and support that have contributed to these published results.

Conflict of interest

The authors declare no conflict of interest.

Keywords: cyclophanes, hydrogen bonds, polymer, self-assembly, supramolecular

[1] L. Brunsveld, B. J. B. Folmer, E. W. Meijer, R. P. Sijbesma, *Chem. Rev.* **2001**, *101*, 4071–4098.
[2] L. Yang, X. Tan, Z. Wang, X. Zhang, *Chemical Reviews* **2015**, *115*, 7196-7239.
[3] aG. Vantomme, E. W. Meijer, *Science* **2019**, *363*, 1396–1397; bJ.-M. Lehn, *Progress in Polymer Science* **2005**, *30*, 814–831.
[4] T. F. A. De Greef, M. M. J. Smulders, M. Wolffs, A. P. H. J. Schenning, R. P. Sijbesma, E. W. Meijer, *Chem. Rev.* **2009**, *109*, 5687–5754.
[5] aM. M. J. Smulders, M. M. L. Nieuwenhuizen, T. F. A. de Greef, P. van der Schoot, A. P. H. J. Schenning, E. W. Meijer, *Chemistry – A European Journal* **2010**, *16*, 362–367; bR. B. Martin, *Chem. Rev.* **1996**, *96*, 3043-3064.
[6] D. Zhao, J. S. Moore, *Org. Biomol. Chem.* **2003**, *1*, 3471–3491.
[7] aC. Kulkarni, E. W. Meijer, A. R. A. Palmans, *Acc. Chem. Res.* **2017**, *50*, 1928–1936; bC. Kulkarni, S. Balasubramanian, S. J. George, *ChemPhysChem* **2013**, *14*, 661–673; cN. M. Casellas, S. Pujals, D. Bochicchio, G. M. Pavan, T. Torres, L. Albertazzi, M. García-Iglesias, *Chem. Commun.* **2018**, *54*, 4112–4115.
[8] D. E. Fagnani, M. J. Meese, Jr., K. A. Abboud, R. K. Castellano, *Angew. Chem. Int. Ed.* **2016**, *55*, 10726–10731.
[9] W. R. Henderson, D. E. Fagnani, J. Grolms, K. A. Abboud, R. K. Castellano, *Helv. Chim. Acta* **2019**, *102*.
[10] D. B. Korlepara, W. R. Henderson, R. K. Castellano, S. Balasubramanian, *Chem. Commun.* **2019**, *55*, 3773–3776.
[11] aJ. Jadzyn, M. Stockhausen, B. Zywucki, *The Journal of Physical Chemistry* **1987**, *91*, 754-757; bK. Pralat, J. Jadzyn, S. Balanicka, *The Journal of Physical Chemistry* **1983**, *87*, 1385-1390; cJ. Nochebuena, C. Cuautli, J. Ireta, *PCCP* **2017**, *19*, 15256–15263; dR. Q. Albuquerque, A. Timme, R. Kress, J. Senker, H.-W. Schmidt, *Chem. Eur. J.* **2013**, *19*, 1647–1657; el. A. W. Filot, A. R. A. Palmans, P. A. J. Hilbers, R. A. van Santen, E. A. Pidko, T. F. A. de Greef, *J. Phys. Chem. B* **2010**, *114*, 13667–13674.
[12] W. R. Henderson, Y. Zhu, D. E. Fagnani, G. Liu, K. A. Abboud, R. K. Castellano, *J. Org. Chem.* **2020**, *85*, 1158–1167.
[13] H. Sun, C. A. Hunter, E. M. Llamas, *Chem. Sci.* **2015**, *6*, 1444–1453.
[14] aM. Wegner, D. Dudenko, D. Sebastiani, A. R. A. Palmans, T. F. A. de Greef, R. Graf, H. W. Spiess, *Chemical Science* **2011**, *2*, 2040-2049; bP. J. M. Stals, J. C. Everts, R. de Bruijn, I. A. W. Filot, M. M. J. Smulders, R. Martin-Rapun, E. A. Pidko, T. F. A. de Greef, A. R. A. Palmans, E. W. Meijer, *Chem. Eur. J.* **2010**, *16*, 810–821; cD. Kluge, J. C. Singer, J. W. Neubauer, F. Abraham, H. W. Schmidt, A. Fery, *Small* **2012**, *8*, 2563-2570.
[15] J. Buendía, J. Calbo, F. García, J. Aragó, P. M. Viruela, E. Ortí, L. Sánchez, *Chem. Commun.* **2016**, *52*, 6907–6910.
[16] aS. Ehrlich, J. Moellmann, S. Grimme, *Acc. Chem. Res.* **2013**, *46*, 916–926; bJ. Antony, R. Sure, S. Grimme, *Chem. Commun.* **2015**, *51*, 1764–1774.
[17] B. Qu, Y. Ma, Q. Ma, X. Liu, F. He, C. Song, *J. Org. Chem.* **2009**, *74*, 6867–6869.
[18] H. J. Reich, D. J. Cram, *J. Am. Chem. Soc.* **1969**, *91*, 3527–3533.
[19] P. Hobza, H. L. Selzle, E. W. Schlag, *J. Am. Chem. Soc.* **1994**, *116*, 3500-3506.
[20] aK. Sako, T. Meno, T. Shinmyozu, T. Inazu, H. Takemura, *Chem. Ber.* **1990**, *123*, 639–642; bH. Dodziuk, S. Szymański, J. Jaźwiński, M. E. Marchwiany, H. Hopf, *J. Phys. Chem. A* **2010**, *114*, 10467–10473.
[21] V. A. Davankov, *Chirality* **1997**, *9*, 99–102.

10.1002/chem.202003909

WILEY-VCH

FULL PAPER

Entry for the Table of Contents

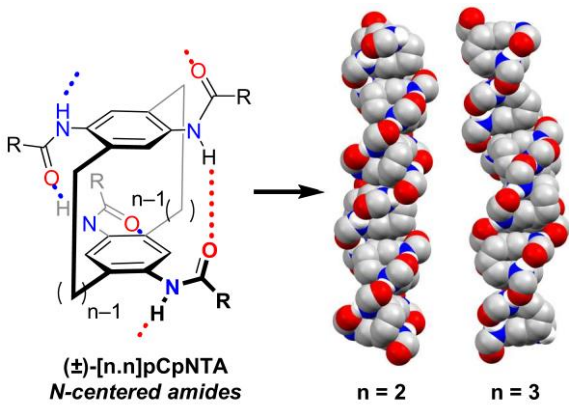

isodesmic supramolecular polymerization
N-centered assembly > C-centered assembly

Cyclophane supramolecular polymers: [n.n]Paracyclophanes equipped with four anilide (*N*-centered amide) hydrogen bonding units (**[n.n]pCpNTA**) self-assemble by an isodesmic mechanism to give supramolecular polymers. The elongation constant for **[n.n]pCpNTA** assembly is two orders of magnitude larger than previously described **[n.n]pCpTAs** with *C*-centered amides.

Institute and/or researcher Twitter usernames: @UFChemistry, @CastellanoLabUF